Journal of Microscopy, Vol. 232, Pt 3 2008, pp. 629–633
Received 20 July 2007; accepted 30 April 2008

Investigation of properties of electrochemically synthesized iron oxide nano-powders

L.J. VULIĆEVIĆ*, N. IVANOVIĆ†, N. POPOVIĆ†, M. NOVAKOVIĆ†, M. POPOVIĆ†, M. MITRIĆ†, V. ANDRIĆ† & D. BABIĆ†

**Technical Faculty Čačak, Svetog Save 65, 32000 Čačak, Serbia*
†Institute of Nuclear Sciences, 'VINČA', P.O. Box 522, 11001 Belgrade, Serbia

Key words. Electrochemical synthesis, Fe oxides, morphology, nano-powders, properties, structure.

Summary

Nano-sized powders of iron oxides have been synthesized electrochemically at temperatures in the range of 295–361 K, and current densities in the range of 200–1000 mA dm^{-2}. The structure and morphology of the powders were investigated by X-ray diffraction and scanning electron and transmission electron microscopy techniques. Their infrared absorption spectra, specific heat $C_p(T)$ and magnetic susceptibility $\chi(T)$ temperature dependences are also determined. The obtained powders consist of two phases, each possessing distinguished characteristics: the one formed of large plates and the other of whiskers. By appropriate adjustment of the synthesis conditions, it is possible to change features and relative abundances of the two phases, and that way to control morphology and other powder properties. Relaxation and transformation of the phases under external influences was also investigated, and the optimal procedure for preparation and stabilization of iron oxide nano-sized powders with desired characteristics was established.

Introduction

The fact that their properties differ from those of bulk materials in many aspects makes iron oxide nano-particles interesting both from a practical and a theoretical point of view (Cornell & Schwertmann, 1996). Below a critical diameter d, which is usually between 10 and 100 nm, they contain a single magnetic domain, and attain the super-paramagnetic regime (Mørup, 1992). These are commonly used as ferro fluids, biomedical materials, catalysts or for magnetic recording (Cornell & Schwertmann, 1996). The relationship between the structure and magnetic properties of iron oxides and their behaviour under heating are important also in geophysics (de Boer & Dekkers, 2001). The general formulae of magnetite and maghemite can be written as: $Fe^{3+}[Fe^{2+}_{1-y}\ Fe^{3+}_{1-y}\ Fe^{3+}_{1,67y}{}^{***}_{0.33y}]\ O_{4-y}$ (***-vacancies, $y = 0$ for pure magnetite, $y = 1$ for pure maghemite) (de Boer & Dekkers, 2001). Although they have similar magnetic properties, maghemite is chemically and thermally more stable and possesses higher electrical resistivity. Magnetite can be synthesized using various procedures (Goya *et al.*, 2003), including the EC method (Ying *et al.*, 2002; Vulićević *et al.*, 2006). The objective of this work is to examine the conditions essential for the EC synthesis of magnetite powders with specific characteristics, and to relate them to their grain size and morphology.

Materials and methods

A glass vessel filled with a solution of sodium chloride in deionized water, with two rectangular low-carbon steel plate electrodes with a separation of about 3 cm, was used as the EC cell. The synthesis conditions, XRD estimated lattice constants and crystallites size and SEM and TEM estimated diameters of smallest grains in the samples are presented in Table 1. We present the results only for powders that show a noticeable deviation from a trend in morphology or some other measured property with synthesis conditions. The synthesis duration (30–60 min) was long enough to produce a sufficient amount of powder but short enough to avoid significant changes in the initial conditions in the EC cell. To reduce further aging, as-obtained filter cakes were washed with deionized water until their conductivity declined below 10 μS cm^{-1}.

X-ray diffractograms were obtained by a Philips 1051 diffractometer (Philips, Eindhoven, the Netherlands), using Cu K_α radiation and Ni filter, in the 2θ angle range of 10–90°, with steps of 0.05°. Scanning electron micrographs (SEM)

Correspondence to: N. Ivanović. Tel: +381 11 2458-222/434; fax: +381 11 344-01-00; e-mail: nivanov@vin.bg.ac.yu

Table 1. Synthesis conditions, lattice constant (a), SEM estimated diameter range of the smallest particles (d_{min}) and XRD estimated crystallite size (d_{cr}) of the investigated powders.

Sample	J (mA dm^{-2})	T (K)	a (nm)	d_{min} (nm)	d_{cr} (nm)
1	200	293	0.8364	110–150	8
2	200	333	0.835	30–50	18
				*10–30	
3	200	361	0.8388	55–75	34
4	500	333	0.832	110–150	18
5	1000	333	0.837	15–30	20
6	1000	361		40–70	
				*10–30	

J – current density; T – temperature, in the EC cell during the synthesis.
*TEM estimated values.

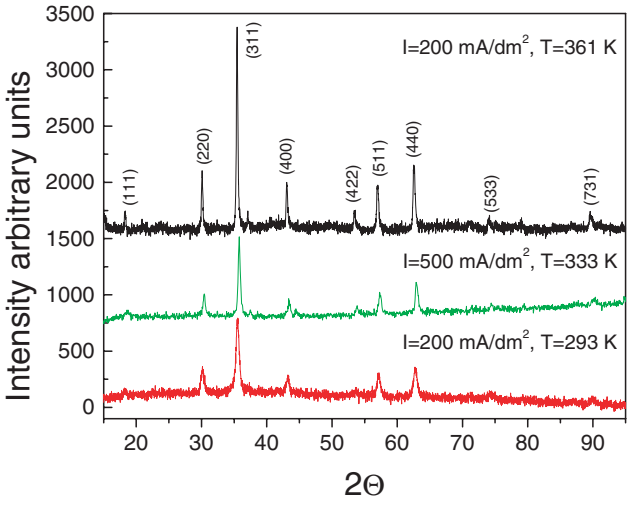

Fig. 1. XRD diffractograms of samples 1, 3 and 4. The indexed phase is magnetite.

were attained with a JOEL, JSM-35 instrument, using a 25 keV electron beam energy and a zero tilt angle. Transition electron micrographs (TEM) were acquired using a Philips EM 400 instrument (Philips) at an operating voltage of 120 kVm, with samples deposited on a carbon-coated copper grid. The IR absorption spectra were recorded at room temperature (RT) in the range 4000–250 cm^{-1}, by a Perkin-Elmer 983G instrument (Perkin-Elmer Optoelectronic, Fremont, CA, USA), using KBr pellets. The specific heat $C_p(T)$ was measured under an N_2 atmosphere, between 320 and 770 K, at a scanning rate of 10 K min^{-1}, by a computer-controlled Perkin-Elmer DSC-2 instrument. Aluminium sample holders and a sapphire standard were used. $C_p(T)$ is determined from $C_p = \frac{W_s \cdot D_s}{W \cdot D} \cdot C_{ps}$, with an error of about ±2%. W_s, D_s and C_{ps} stand, respectively, for the mass, obtained signal and specific heat of the standard at a particular temperature, where W and D are measured values of a sample. The temperature dependence of the magnetic susceptibility $\chi(T)$ was measured in air, with an applied magnetic field strength of 5440 A m^{-1}, by the modified Faraday's method.

Results and discussion

XRD diffractograms of samples 1, 3 and 4 (Fig. 1) show that magnetite is the dominant compound in the produced powders over the entire range of current densities and temperatures used in experiments. Diffuse background below the main diffractogram peaks (see Fig. 1 and Vulićević *et al.*, 2006) implies presence of some amorphous material in samples 1 and 5. Departures of the lattice constant values of various powders (Table 1) from that of perfectly ordered magnetite ($a = 0.8396$ nm) indicate deviations in their stoichiometry.

The grain morphology of the powders (Figs 2 and 3) varies considerably with the producing conditions, but two major phases can be distinguished. One is made of large plate-like grains and presumably emerges from lepidocrocite (γ–FeOOH). The other one, the 'whiskers' phase, most likely develops from goethite (α–FeOOH), as the intermediate phase. Sample 1 consists mainly of particles ranging from 1.5 to 75 μm (Fig. 2(a)), with morphology that is quite different from that seen in other samples. Under higher magnification, a distinct group of particles, with d around 500 nm, were also detected. Small grains of about 100 nm in size grow at the cross section of the large particles' surfaces, illustrating mechanism of formation of large particles from the smaller ones. Sample 2 is homogenous composed of small grains with d ranging from 30 to 50 nm (Fig. 2(b)). A relatively small number of particles has d of about 150 nm, the larger particles being the agglomerates of the smaller ones. Sample 3 also consists of the small grains, but their prevailing form is somewhat different from those observed in other samples (Fig. 2(c)). The grain distribution is narrow, most of the particles having a d of about 150 nm, and the smallest among them, in the range of 55–75 nm. The large plates' phase is not fully developed, although some very isolated regular large shapes (d of approximately 1000 nm) have been observed. Larger particles (d of approximately 450 nm) are formations built from the smaller ones. Few fibres with d of approximately 150 nm are also observed. Sample 4 also consists predominately of small grains (Fig. 2(d)), but the plate-like forms and fibre-dendrite forms preferably growing on and around the plate-like ones, are clearly visible. The average fibre diameter $<d>$ is about 110 nm, and $<d>$ of the plate-like structure is about 1500 nm. The observed ball-like grains, with $<d>$ around 150 nm, could be fibre cross sections or their ends. The large plate-like phase, and the whiskers (fibre–dendrite), are present also in sample 5 (Fig. 2(e)). Large crystallites have several different shapes: completely irregular, partially regular with well-defined angles and d = 300–800 nm, and regular disks with d of approximately 800 nm, indicating that under the used synthesis conditions, full development of the large

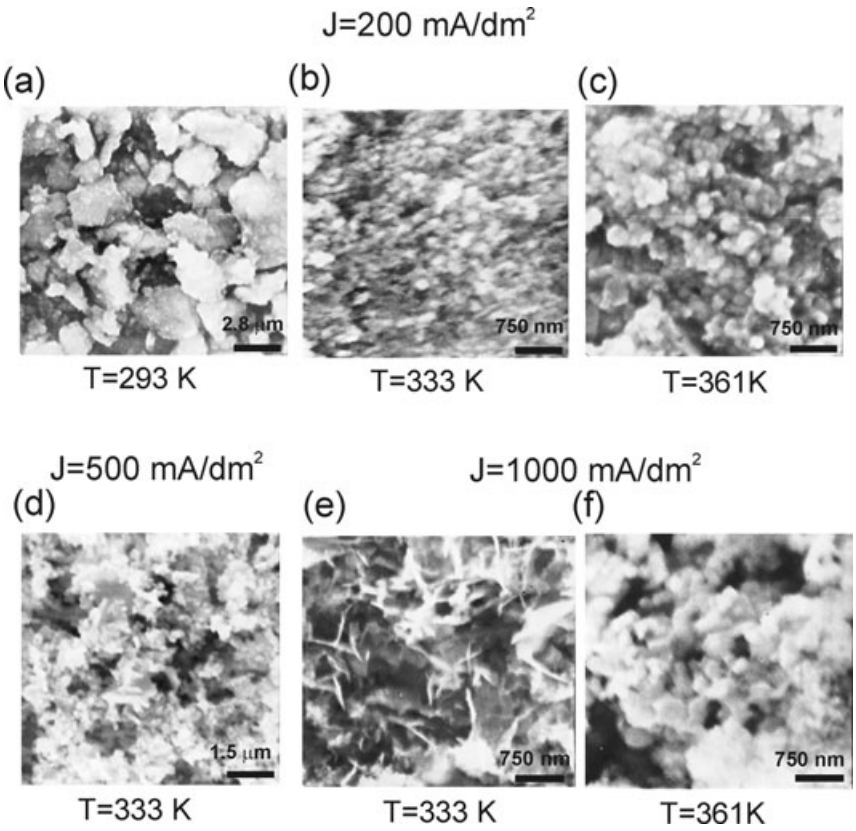

Fig. 2. SEM images: (a) sample 1, (b) sample 2, (c) sample 3, (d) sample 4, (e) sample 5 and (f) sample 6.

plate-like phase requires a grain diameter of about 800 nm. A great variety of needle-like structures is found, as standing alone, or forming complex bundles and dendrite forms on the plate-like structure surfaces. $<d>$ of a single needle ranges between 30 and 80 nm, although the needles with d as small as 15 nm have been found. Sample 6 also comprises small particles accompanied with some polygonal and plate-like formations (Fig. 2(f)). For the small particles $d = 40$–70 nm, and for their larger agglomerates, d goes up to 400 nm.

A more detailed powder morphology of samples 2 and 6 is shown in the bright-field TEM images (Figs 3(a) and (b), respectively). The particles in sample 2 are rather isotropic and have a relatively uniform size distribution, with $<d>$ in the range of 10–30 nm. The larger structures are mainly the agglomerates of the smaller ones. The TEM image of sample 6 (Fig. 3(b)) shows a structure similar to the one of sample 2. It is composed of homogenous and nearly spherical small grains, but in this sample the bundles of fibres have been also observed.

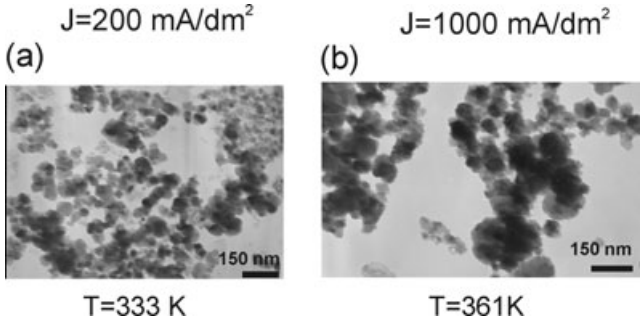

Fig. 3. TEM images of (a) sample 2 and (b) sample 6.

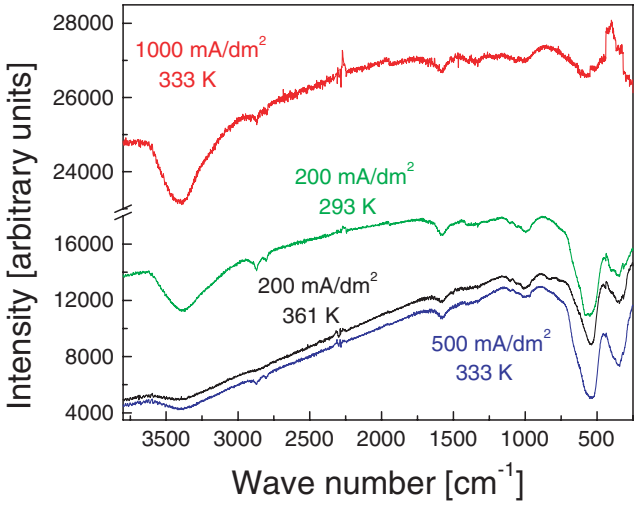

Fig. 4. IR spectra of samples 1, 3, 4 and 5.

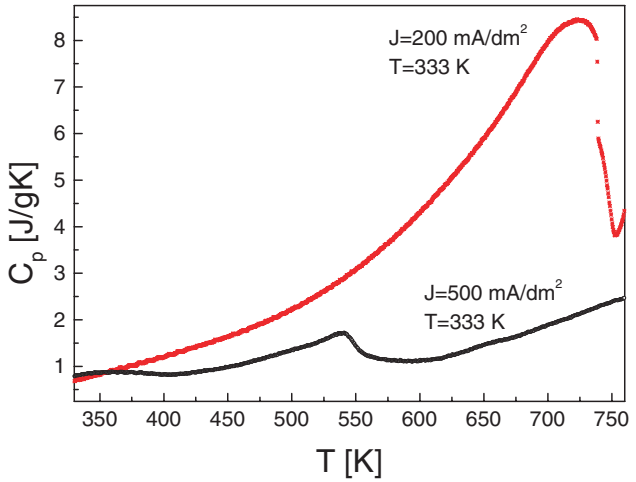

Fig. 5. Specific heat $C_p(T)$ dependence of samples 2 and 4.

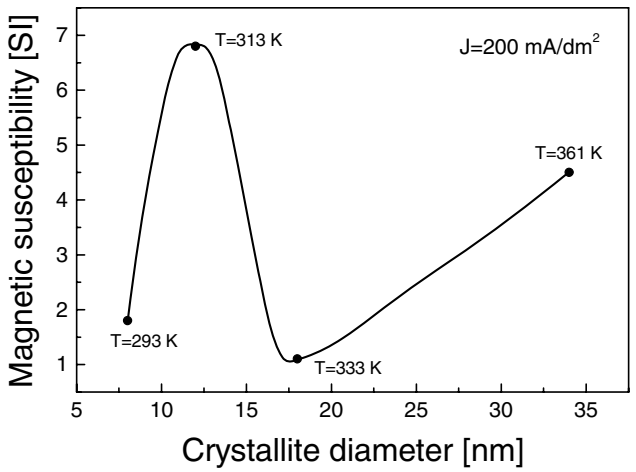

Fig. 6. Crystallite size dependence of magnetic susceptibility of powders obtained at $J = 200$ mA dm^{-2} and $T = 293$, 313, 333 and 361 K. The line is sketched to guide the eye.

The results suggest that T during the synthesis predominately determines the crystallite size (d_{cr}), and that both high T and high J reduce agglomeration. However, these dependences are not simple and some irregularities are observed in the trends, particularly around $T = 333$ K and $J = 500$ mA dm^{-2} accompanied with deviations in optical, calorimetric and magnetic characteristics of the powders obtained in that range of synthesis conditions.

The IR spectra of samples 1, 3, 4 and 5 are presented in Fig. 4. The spectra of samples 1, 3 and 4 are quite similar comprising the pronounced magnetite bands around 360 and 560 cm^{-1}, the exact position of which depending on sample stoichiometry (Gotić & Musić, 2007). The adsorbed water peaks around 3400 cm^{-1} (O–H stretching) and 1600 cm^{-1} (O–H bending) (Gotić & Musić, 2007) are especially pronounced in samples 1 and 5. The presence of small amounts of α- and γ-FeOOH phases in the samples is exposed through the banding bands of the OH groups existing in the hydroxides' crystal structures, appearing in the spectra around 1100 and 1380 cm^{-1} (Nasrazadani, 1997). The weak structure around 2900 cm^{-1} is probably due to the stretching motions of the hydroxides' OH groups (Gotić & Musić, 2007). The sample 5 pattern differs significantly in the region of wave vectors related to the magnetite crystal structure. The reasons for this could be a significant amount of an amorphous phase, detected by XRD measurements (Vulićević *et al.*, 2006), and perhaps a deviation from stoichiometry, producing a structure between the magnetite and the maghemite one.

The results of specific heat $C_p(T)$ measurements of samples 2 and 4 are presented in Fig. 5. Although the C_p(RT) values of the two samples are similar (between 0.7 and 0.8 Jg^{-1}K^{-1}) and close to the literature value (Weidenfeller *et al.*, 2002), their temperature characteristics differ greatly. Sample 2 has a large heat capacity, undergoing the phase transition at T_c between 700 and 750 K, close to the Curie temperature of magnetite (approximately 850 K). Sample 4 has considerably smaller heat capacity, and less pronounced phase transition, taking place at a T_c between 530 and 550 K. These discrepancies have their origin in different grain size distributions and the extent of agglomeration in the two samples, resulting in different magnetic structures of the grains, and a different inter-grain magnetic interaction. To obtain more information on magnetic structure of the powders, we have measured temperature dependence of their magnetic susceptibility, $\chi(T)$. The results obtained for various samples are quite different (Vulićević *et al.*, 2006). The χ(RT) dependence on the crystallite size, presented in Fig. 6, shows the super-paramagnetic transition for a crystallite diameter in the range between 13 and 20 nm.

Conclusions

The results of the presented investigations infer that relative amount and features of the two quite different phases that occur during the EC synthesis of magnetite nano-powders can be regulated by appropriate combinations of temperature and current density in the EC cell. One of the phases consists of large plate-like grains, which, when fully developed, have a diameter around 800 nm, and emerges from lepidocrocite. The other is composed of grains with dimensions in the range of 10–100 nm, and originates from goethite, as the intermediate phase. Various modes of agglomeration and interaction of, and between, the two phases have been observed, providing formation of some quite extraordinary structures, such as needles, their bundles and dendrites, which have been found as stand-alone structures or grown on the surfaces of the large plates. By choosing the appropriate phase, or the relative amount of the two, it is possible to control structure, grain morphology, magnetic, electrical and optical

characteristics of the EC produced nano-sized powders of Fe oxides, which could be of a great importance for their practical applications.

Acknowledgement

The financial support of the Ministry of Science and Environmental Protection of the Republic of Serbia under the grant 141009B is gratefully acknowledged.

References

Cornell, R.M. & Schwertmann, U. (1996) *Iron Oxides*. VCH Verlagsgesellschaft, Weinheim.

de Boer, C.B. & Dekkers, M.J. (2001) Unusual thermomagnetic behaviour of haematites: neoformation of a highly magnetic spinel phase on heating in air. *Geophys. J. Int.* **144**, 481–494.

Gotić, M. & Musić, S. (2007) Mössbauer, FT-IR and FE SEM investigation of iron oxides precipitated from $FeSO_4$ solutions. *J. Mol. Srtruct.* **834–836**, 445–453.

Goya, G.F., Berquo, T.S. & Fonseca, F.C. (2003) Static and dynamic magnetic properties of spherical magnetite nanoparticles. *J. Appl. Phys.* **94**, 3520–3528.

Mørup, S. (1992) Mössbauer studies of isolated and interacting ultra fine magnetic particles. *Magnetic Properties of Fine Particles* (ed. by J.L. Dormann & D. Fiorani), pp. 125–190. Delta Series, North Holland, Amsterdam.

Nasrazadani, S. (1997) The application of infrared spectroscopy to a study of phosphoric and tannic acids interactions with magnetite (Fe_3O_4), goethite (α-FeOOH) and lepidocrocite (γ-FeOOH). *Corr. Sci.* **39**, 1845–1859.

Vulićević, Lj., Ivanović, N., Maričić, A., Vučković, A., Popović, N. & Vardić, S. (2006) Structural, magnetic, and electrical characteristics of metastable Iron oxide nano-sized powders. *Mater. Sci. Forum* **518**, 113–119.

Weidenfeller, B., Höfer, M. & Schilling, F. (2002) Thermal and electrical properties of magnetite filled polymers. *Composites: Part A* **33**, 1041–1053.

Ying, T.-Y., Yiacomi, S. & Tsouris, C. (2002) An electrochemical method for the formation of magnetite particles. *J. Disp. Sci. Technol.* **23**, 569–576.

